



Current Understanding of Nonaqueous Electrolytes for Calcium-Based Batteries

Aaron M. Melemed,^[a] Aliza Khurram,^[a] and Betar M. Gallant^{*[a]}

Calcium metal batteries are receiving growing research attention due to significant breakthroughs in recent years that have indicated reversible Ca plating/stripping with attractive Coulombic efficiencies (90–95 %), once thought to be out of reach. While the Ca anode is often described as being surface film-controlled, the ability to access reversible Ca electrochemistry is highly electrolyte-dependent in general, which affects both interfacial chemistry on plated Ca along with more fundamental Ca^{2+}/Ca redox properties. This minireview describes recent

progress towards a reversible Ca anode from the point of view of the most successful electrolyte chemistries identified to date. This includes, centrally, what is currently known about the Ca^{2+} solvation environment in these systems. Experimental (physico-chemical and spectroscopy) and computational results are summarized for the two major solvent classes – carbonates and ethers – that have yielded promising results so far. Current knowledge gaps and opportunities to improve fundamental understanding of Ca^{2+}/Ca redox are also identified.

1. Introduction

Advances in the chemical underpinnings of today's batteries will have a significant impact on the future of energy storage.^[1] Lithium-ion (Li-ion) batteries based on graphite anodes and transition-metal-oxide cathodes have proven to be capable devices for consumer electronics and, increasingly, for electric vehicles (EV).^[2] However, mass-market EV adoption and broader storage applications remain constrained by current limitations of Li-ion. These include limited capacities of oxide intercalation cathodes (~150–280 mAh/g_{practical}) and, secondarily, of graphite (372 mAh/g_{theoretical}); limited commercial cell-level energy densities (~260 Wh/kg and 700 Wh/L); among other challenges.^[1–4] Although replacement of graphite with Li metal would significantly increase gravimetric and volumetric energy, Li battery development is impeded by the tendency to form Li dendrites during cycling, an unacceptable safety hazard. Sodium (Na) and magnesium (Mg) anodes have been explored,^[5–9] but these metals have higher potentials voltages than Li (−3.04 V vs. SHE) and thus yield lower total cell voltages than Li. In addition, Na batteries have been hampered by dendrites and low gravimetric energy densities.^[5,6] Meanwhile, Mg batteries experience obstacles related to the highly-polarizing nature of the divalent Mg^{2+} , issues with electrolyte compatibility and safety, and low energy densities as well.^[7–9]

Compared to other candidate metals, calcium (Ca) offers several potential advantages, particularly where scalability and sustainability are concerned (Figure 1; also discussed in detail by others^[10–12]). At 41,500 ppm, Ca is the fifth-most abundant element in the earth's crust with over 2000× the abundance of

Li.^[13] Additionally, Ca offers attractive electrochemical metrics. The electrochemical potential, at −2.87 V vs. SHE, is only 170 mV more positive than Li, leading to the possibility of similar full cell voltages. Although Ca has an atomic mass 6× higher than Li, its divalence, along with only moderately larger ionic radius (1.00 vs. 0.72 Å for Ca^{2+} vs. Li^+) yields a theoretical volumetric capacity of 2073 mAh/cc (vs. 2062 mAh/cc_{Li}).^[11] Compared to Mg^{2+} , the larger ionic radius of Ca^{2+} reduces charge polarization, potentially improving ion transport through solution and in the solid-state.^[12,14,15] Furthermore, Ca has a significantly higher melting temperature than Li (842 °C vs. 181 °C) and thus potentially improved safety. A few studies have indicated the possibility of Ca to deposit smoothly in some electrolytes,^[16,17] even at current densities up to 1 mA/cm²,^[17] potentially avoiding dendrite issues. Early practical implementation of Ca batteries may focus on niche utilization where safety and portability are paramount, such as naval or space applications, while opening the door to longer-term development for electrified transportation.

In spite of the above, development of Ca-based batteries is still in its infancy due to basic chemical limitations. Unlike Li, which spontaneously forms a chemically-protective, electronically-blocking yet Li^+ -conducting solid electrolyte interphase (SEI) in contact with organic electrolytes, the native SEI formed on Ca in most organic electrolytes consists of phases (e.g. CaO , CaCO_3 , Ca(OH)_2 , and Ca alkoxides) that are thought to be fully Ca^{2+} -blocking. As a result, a reversible metallic Ca anode that can strip and plate with even modest Coulombic efficiency (CE) was thought for many years to be out of reach. Several potential Ca^{2+} intercalation cathodes^[18–27] and high-capacity conversion-type (O_2 , S) cathodes^[28–30] have been explored, but overall, the lack of an electrochemically reversible Ca anode has hampered scientific progress of Ca and Ca-ion systems.

In the past several years, however, several groundbreaking studies reported reversible deposition and dissolution of Ca in select organic electrolytes for the first time,^[16,17,31,32] prompting a dramatic renewal of interest. Although fundamental under-

[a] A. M. Melemed, A. Khurram, Prof. B. M. Gallant
Department of Mechanical Engineering,
Massachusetts Institute of Technology,
77 Massachusetts Avenue, Cambridge, MA 02139, USA
E-mail: bgallant@mit.edu

An invited contribution to a Special Collection on Electrolytes for Electrochemical Energy Storage

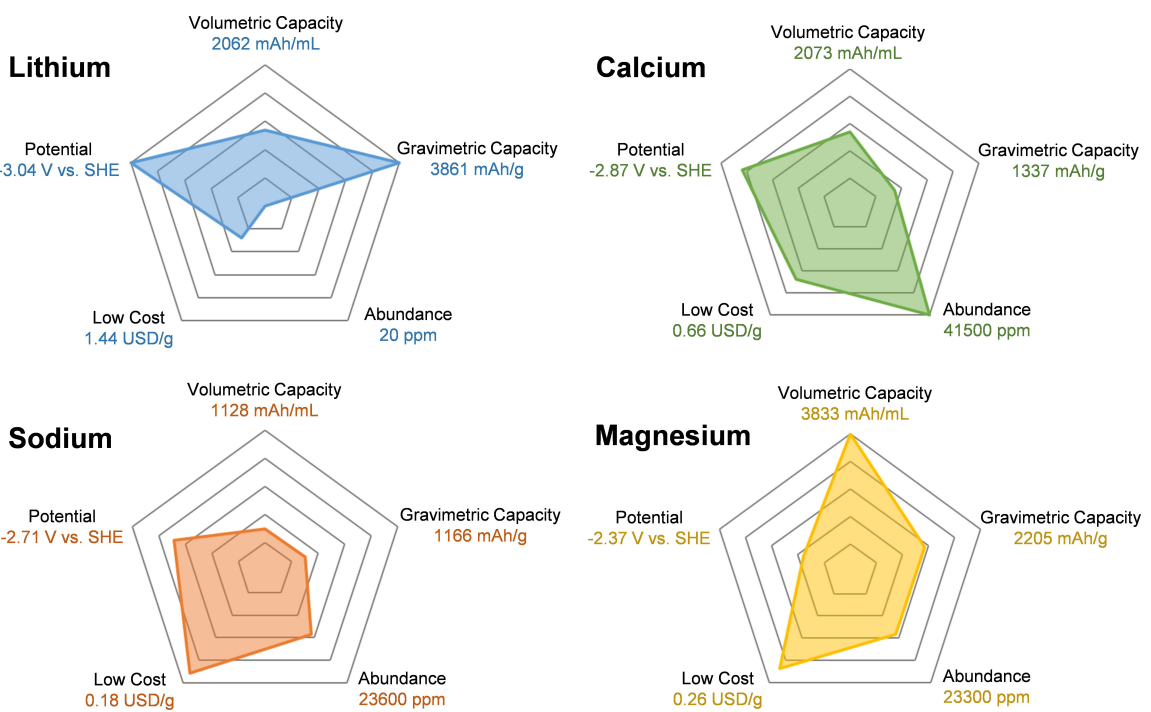


Figure 1. Performance metrics of metal anodes. Radar plots charting useful metrics to assess theoretical performance, cost, and manufacturability of metal anodes. Cost estimates are based on current prices for 99% pure, minimally processed metals from Sigma-Aldrich or Alfa Aesar.

standing is still needed, these advances point towards the substantially enabling – or disabling – role of the electrolyte chemistry, along with the derived solid-state chemistry comprising the SEI on Ca. While previous reviews covered aspects of multivalent battery systems including Mg^[15,33–35] and Ca (including Ca²⁺ host materials and performance of Ca anodes),^[10–12] there is still a significant need for improved understanding of Ca²⁺ in the liquid environment: how solvation chemistries affect electrochemical behaviors, SEI, and reversi-

bility. In this mini-review, we summarize current knowledge of organic Ca electrolytes and provide a focused survey of current research needs.



Aaron Melemed is a graduate student in the Department of Mechanical Engineering at the Massachusetts Institute of Technology (MIT). He obtained his B.S. of Mechanical Engineering from Purdue University in 2015, then spent several years working in industry. His research interests include solid-electrolyte interphases and multivalent batteries.



Aliza Khurram is a PhD candidate in the Department of Mechanical Engineering at the Massachusetts Institute of Technology (MIT). She obtained her B.S. in Physics and Mathematics from Bates College in 2015, and her M.S. in Mechanical Engineering from MIT in 2017. Her research interests include high-capacity conversion cathodes for beyond-Li ion batteries (e.g.: Li-gas batteries) and alternative metal-anode materials.



Betar M. Gallant is the ABS Career Development Assistant Professor in the Department of Mechanical Engineering at MIT. She obtained her SB (2008), SM (2010), and PhD (2013) from the same department, and was a Kavli Nanoscience Institute Prize Postdoctoral Fellow at Caltech in the Division of Chemistry and Chemical Engineering from 2013–2015. Her research group at MIT focuses on Li battery technologies, including advanced gas-solid conversion cathodes, Li solid electrolyte interphase characterization, and fluoridation of oxide cathodes; beyond-Li anodes (e.g. Ca); and CO₂ capture and conversion. She is the recipient of an MIT Bose Fellows Award (2017), Army Research Office Young Investigator Program Award (2019), and Scialog Fellow in Energy Storage (2019).

2. Early Understanding of Ca Anodes and Ca^{2+} Solvation in Primary Batteries

Concerted interest in nonaqueous Ca electrochemistry began in 1980 with Staniewicz's study of the Ca-thionyl chloride ($\text{Ca}-\text{SOCl}_2$) primary battery.^[36] The attraction of a Ca analogue to the successful $\text{Li}-\text{SOCl}_2$ system was safety, due to Ca's higher melting temperature and apparent lack of electrodeposition upon accidental cell reversal, a safety issue with $\text{Li}-\text{SOCl}_2$ systems.^[37] In fact, a ~40 V overpotential was required to deposit Ca from 1.3 M $\text{Ca}(\text{AlCl}_4)_2/\text{SOCl}_2$ at <10% CE before surface passivation terminated plating.^[38] Furthermore, within a full cell construction, the Ca anode was found to corrode through continuous reaction of Ca and/or the CaCl_2 SEI with electrolyte. As a result, the CE during battery discharge was only ~50%,^[36] and the initial cell operated at a low rate of 1 mA/cm².

Over the next decade, significant efforts were expended on optimizing electrolyte properties to improve performance. A correlation between ionic conductivity and capacity was identified early on; higher ionic conductivities minimized transport limitations at the cathode arising from buildup of insulating discharge products.^[36,38] $\text{Ca}(\text{AlCl}_4)_2$ concentration was found to play a crucial role: as concentration increased from 0.38 to 1.2 M at 30 °C, ionic conductivity increased (~1.5 to ~6.5 mS/cm),^[38] after which viscosity became an issue.

Additional studies examined effects of SO_2 gas additive, which further increased ionic conductivity.^[39–42] For example, adding 10% (v/v) SO_2 to 1.3 M $\text{Ca}(\text{AlCl}_4)_2/\text{SOCl}_2$ led to an increase from ~6 to ~11 mS/cm at 25 °C.^[39] SO_2 was also found to increase capacity, though this was proposed to be a physical rather than chemical effect resulting largely from physical release of SO_2 at the cathode during discharge, increasing porosity and postponing cathode passivation.^[40,43] The reasons underlying improvements in ionic conductivity were not well understood until fundamental studies were conducted into Ca^{2+} solvation in the analogous Ca-sulfuryl chloride (SO_2Cl_2) system.

In 1982, Binder *et al.* reported the $\text{Ca}-\text{SO}_2\text{Cl}_2$ primary battery as a potential improvement to $\text{Li}-\text{SO}_2\text{Cl}_2$. $\text{Ca}-\text{SO}_2\text{Cl}_2$ cells showed discharge voltages ~0.4 V higher than $\text{Ca}-\text{SOCl}_2$ (~3.2 vs. 2.8 V, 0.1 mA/cm²)^[44] but ionic conductivities were significantly lower.^[45] Subsequent studies probed the electrolyte environment using nuclear magnetic resonance (NMR) measurements^[46] and Raman spectroscopy^[47] at varying salt concentrations with SO_2 present at saturation levels. ¹⁷O NMR revealed that O atoms in SO_2Cl_2 normally coordinate Ca^{2+} , as expected given the strong oxophilicity of Ca.^[12] However, added SO_2 molecules preferentially complexed Ca^{2+} by displacing SO_2Cl_2 . ⁴³Ca NMR further revealed a more shielded state of Ca^{2+} with SO_2 present^[46] stemming from closer coordination of Ca^{2+} and the smaller SO_2 . Raman spectroscopy supported these conclusions: a broad band appearing at 1155 cm⁻¹ in SO_2 -saturated electrolyte was attributed to formation of $n\text{SO}_2-\text{Ca}^{2+}$ complexes. n was not specified therein, but a similar band at 1157 cm⁻¹ in $\text{LiAlCl}_4-\text{SOCl}_2$ solutions indicated $n=3$ around

Li^+ .^[48] The improvements in ionic conductivity were thus attributed to displacement of the bulkier SO_2Cl_2 by SO_2 in the cation's solvation sphere, reducing the solvation sheath size and increasing $\text{Ca}^{2+}_{\text{solv}}$ mobility.^[47] However, smaller solvation sheath sizes may imply more strongly-bound solvent molecules, and thus impede desolvation kinetics for certain solvents, as will be discussed further below. It should be noted that the chemical state of the anion, AlCl_4^- , was not widely discussed. The formation of ionic aggregates was proposed to explain some low-temperature and concentration-dependent conductivity trends,^[38] but otherwise, it seems that cation-anion interactions were not assumed to play a major role.

It is also worth noting that the interface in Ca primary batteries containing SOCl_2 or SO_2Cl_2 consisted primarily of CaCl_2 .^[36,45,49] Unlike the Li SEI, which is Li^+ conducting, (Figure 2), CaCl_2 is mostly an anion (Cl^-)-conductor (anion transference number of ~0.9).^[49] The implications of this difference on the nature of interfacial redox mechanisms are potentially significant.^[49] For Li, the essential charge-transfer process upon plating is from $\text{Li}^+_{\text{solv}}/\text{Li}^+_{\text{SEI}}$ and then $\text{Li}^+_{\text{SEI}}/\text{Li}^0$ at the electrolyte and Li interfaces, respectively, where the subscript "SEI" denotes mobile Li^+ . The SEI is (nominally) stable and non-reactive, but is displaced physically to accommodate volume change as Li is plated (or, in reverse, stripped). In contrast, in Ca systems where Cl^- is the mobile ion, the liquid- and solid-state carriers differ. Consequently, the electrolyte-facing redox step upon Ca plating involves precipitation of CaCl_2 , *viz.* [Eq. (1)],



while the Ca-facing redox process involves reduction of non-mobile Ca^{2+} within the CaCl_2 lattice [Eq. (2)].

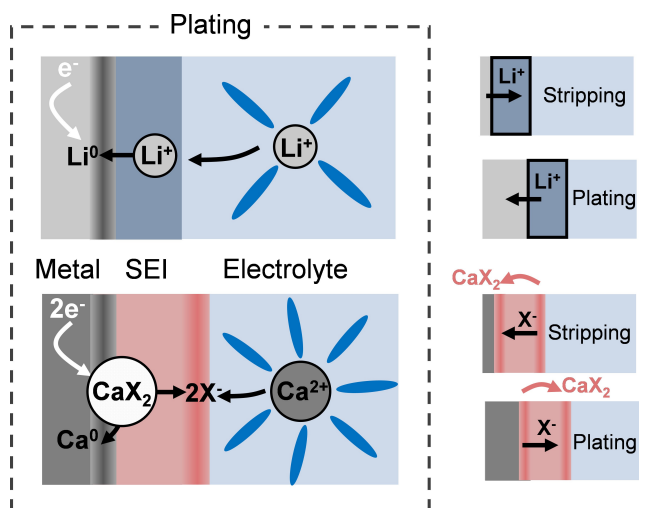
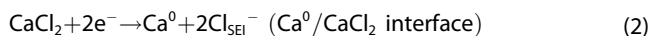


Figure 2. SEI behavior with a cation (Li^+) vs. anion (X^-) conductor. (Left) Li^+ plating with a cation-conductive SEI and Ca^{2+} plating (hypothetical) with an anion-conductive SEI. (Right) Nominal stripping and plating processes. A cation-conductive Li^+ SEI is nominally displaced during cycling, whereas an anion-conductive Ca^{2+} SEI requires active dissolution/precipitation of the SEI at interfaces.



Thus, a dynamic chemical precipitation/dissolution occurs. (Note that plating has not been demonstrated practically with CaCl_2 ; the reverse stripping process, also involving dynamic participation of interfaces, predominates in Ca primary batteries). Given that several SEI-relevant phases observed in successful systems of late (discussed further below) include CaF_2 and CaH_2 , which are reported to be anion-conductors,^[50,51] there is much yet to be learned about the fundamental physical behaviors of Ca interfaces, especially under electrochemical conditions.

Ultimately, while research into the primary $\text{Ca}-\text{SOCl}_2$ and $\text{Ca}-\text{SO}_2\text{Cl}_2$ systems provided a first look into the behavior of Ca^{2+} in nonaqueous solvation environments, anode corrosion and inadequate low-temperature performance hindered further development.^[43] Subsequent Ca-based research shifted away from oxyhalides and towards common organic battery solvents.

3. Successful Ca Plating and Stripping in Carbonate Electrolytes

Poor reversibility of Ca in most battery electrolytes was first illustrated in 1991 when Aurbach *et al.* extensively studied Ca cycling in the common battery solvents γ -butyrolactone (BL), acetonitrile (ACN), tetrahydrofuran (THF), and propylene

carbonate (PC), containing a wide range of salts (LiAsF_6 , LiClO_4 , $\text{Ca}(\text{ClO}_4)_2$, $\text{Ca}(\text{BF}_4)_2$, TBABF_4 , and TBACIO_4).^[52] Cyclic voltammetry (CV) using a Ca working electrode revealed anodic currents corresponding to Ca dissolution to a varying extent in all electrolytes; however, cathodic currents were considerably smaller (*e.g.*, $< 0.5 \text{ mA/cm}^2$ cathodic vs. $\sim 3 \text{ mA/cm}^2$ anodic for 0.5 M $\text{Ca}(\text{ClO}_4)_2$ /BL) and were attributed mainly to electrolyte decomposition. Scanning electron microscopy (SEM) and Fourier-transform infrared (FT-IR) spectroscopy analysis on deposited Ca revealed surface films of insulating organic phases (alkoxide, ester, and carboxylates), and a range of inorganic byproducts (including Ca(OH)_2 , CaCO_3 , CaCl_2) depending on electrolyte. Consequently, the authors concluded that Ca deposition is surface-film controlled, in that fresh deposits readily react with the electrolyte and block subsequent ion flow.

In 2016, the first reversible Ca deposition was demonstrated by Ponrouch *et al.* on stainless steel plungers at elevated temperatures (75–100 °C). The electrolyte was $\text{Ca}(\text{BF}_4)_2$ with 1:1 (v-v) ethylene carbonate (EC):PC.^[16] It was mentioned that higher temperatures support breakage of ion pairs in general. Two additional salts – $\text{Ca}(\text{ClO}_4)_2$ and $\text{Ca}[(\text{CF}_3\text{SO}_2)_2\text{N}]_2$ ($\text{Ca}(\text{TFSI})_2$) – were also investigated, but $\text{Ca}(\text{ClO}_4)_2$ was found to be substantially less active, whereas $\text{Ca}(\text{TFSI})_2$ was fully inactive towards Ca deposition even at high temperatures, indicating a special role for $\text{Ca}(\text{BF}_4)_2$. Moreover, the concentration of $\text{Ca}(\text{BF}_4)_2$ was a critical parameter: reduction currents were maximized at 0.45 M (Figure 3a). The ionic conductivity (measured at room temperature) was also found to be a maximum

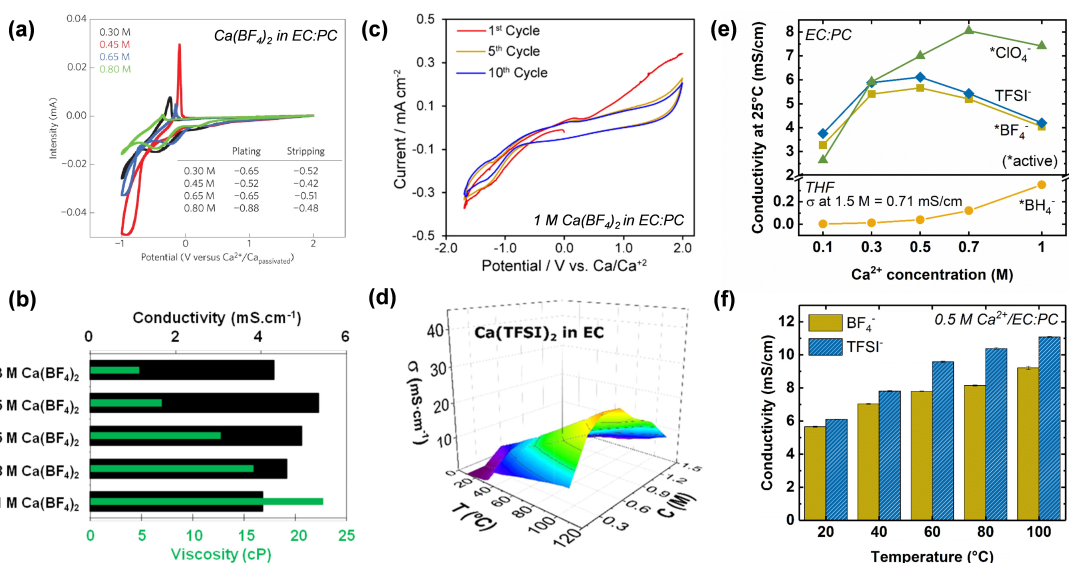


Figure 3. Physico-chemical properties of Ca electrolytes with carbonate solvents. a) CVs showing Ca plating/stripping with $\text{Ca}(\text{BF}_4)_2$ in EC:PC as a function of concentrations at 100 °C and 0.5 mV/s, and b) room-temperature ionic conductivity and viscosity as a function of $\text{Ca}(\text{BF}_4)_2$ concentration in EC:PC. Figures 3a-b reprinted by permission from Springer Nature: Nature Publishing Group, Nature Materials, Ref. [16], Copyright 2016. c) CV with 1 M $\text{Ca}(\text{BF}_4)_2$ in EC:PC (room temp.) at 25 mV/s. Reprinted with permission from Ref. [54]. Copyright 2019, American Chemical Society. d) Ionic conductivity of $\text{Ca}(\text{TFSI})_2/\text{EC}$ electrolyte at varying temperatures and salt concentrations. Reprinted with permission from Ref. [55]. Copyright 2019, American Chemical Society. e) Room-temperature ionic conductivity as a function of salt concentration for EC:PC containing $\text{Ca}(\text{BF}_4)_2$, $\text{Ca}(\text{ClO}_4)_2$, and $\text{Ca}(\text{TFSI})_2$, as well as THF containing $\text{Ca}(\text{BH}_4)_2$. f) Ionic conductivity of 0.5 M $\text{Ca}(\text{BF}_4)_2$ and $\text{Ca}(\text{TFSI})_2$ in EC:PC at varying temperatures. The experimental methods of e-f) were reported previously.^[53] (EC – Acros Organics, 99%; PC – Sigma-Aldrich, 99.7%; THF – Aldrich, 99.9%; $\text{Ca}(\text{BF}_4)_2$ – Apollo Scientific, 95%; $\text{Ca}(\text{ClO}_4)_2$ – Aldrich, unspecified; $\text{Ca}(\text{TFSI})_2$ – Solvionic, 99.5%; $\text{Ca}(\text{BH}_4)_2$ ·2THF – Aldrich, 99.7%). The salts intended for EC:PC were vacuum dried overnight at 120 °C; the water content of EC:PC and THF after 3 days of drying over molecular sieves were each $< 10 \text{ ppm}$.

(5.4 mS/cm) at this concentration (Figure 3 b), after which substantial viscosity increases, attributed to cation-anion pairing, led to a decline. Thus, it was suggested that conditions at which Ca^{2+} mobility is maximized are also most amenable to Ca deposition. Minimizing BF_4^- in the Ca^{2+} solvation sphere was indicated as advantageous for achieving this goal. The SEI formed on deposited Ca from $\text{Ca}(\text{BF}_4)_2$ at 75 °C contained CaF_2 as determined from X-ray diffraction (XRD), as well as solvent-derived organic phases identified by FT-IR; the origin of CaF_2 (whether from fully-dissociated BF_4^- or Ca^{2+} -solvating BF_4^-) is not currently known.

Biria *et al.* recently reported that high temperatures may not be strictly necessary for reversible Ca plating/stripping in carbonates. Utilizing the same champion electrolyte, 1 M $\text{Ca}(\text{BF}_4)_2$ in EC:PC, and a copper working electrode, the authors reported reversibility of ~20 μm deposition thicknesses over several CV cycles at room temperature (Figure 3c).^[54] The Coulombic efficiencies were high (> 95%). However, the reported cathodic current densities were < 0.4 mA/cm², approximately two orders of magnitude lower than those attainable upon Li plating in comparable carbonate electrolyte (~tens of mA/cm²). The areal current density of the original carbonate study^[16] was unknown, making cross-study comparison challenging, but the stark qualitative difference between the two CVs should be noted. However, as discussed later, several systems have recently achieved current densities commensurate with Li by utilizing ether electrolytes,^[17,31,32] while it is not currently clear whether carbonates can do so for Ca. The room-temperature deposits, while containing Ca as indicated by XRD, did not contain crystalline secondary phases such as CaF_2 . Thus, a second open question regarding CaF_2 is whether it plays a functional role and is thus a desirable phase within the SEI (recall that CaF_2 is reported to be an anion conductor, Figure 2), or if it instead forms incidentally at higher temperatures. In addition, this study used a reduction cutoff potential of ~1.7 V, and it should be noted that parasitic side reactions are more prone to occur at lower reduction potentials.

3.1. Ionic Conductivity Trends in Carbonate Electrolytes

More recently, Forero-Saboya *et al.* further investigated physico-chemical properties of $\text{Ca}(\text{TFSI})_2$ in carbonate electrolytes.^[55] A maximum in ionic conductivity vs. concentration – as observed for $\text{Ca}(\text{BF}_4)_2$ originally – also occurs for $\text{Ca}(\text{TFSI})_2$ in EC (~7 mS/cm, 0.5 M, Figure 3d), PC (~6 mS/cm, 0.42 M), and DMF (~20 mS/cm, 0.5 M) at 30 °C. The ionic conductivity maxima scaled monotonically with the solvent donor number (DMF > EC > PC); at higher concentrations, ion-pairing became predominant. The maxima typically occurred in the range 0.4–0.6 M for $\text{Ca}(\text{TFSI})_2$, significantly lower than those of Li^+ -based electrolytes (1–1.2 M).^[56] In addition, ionic conductivity increased monotonically with temperature, which was attributed to the increased breakage of ion pairs as mentioned in the original study.^[16]

To complement the above results, ionic conductivity for the relevant salts ($(\text{Ca}(\text{TFSI})_2$, $\text{Ca}(\text{BF}_4)_2$, and $\text{Ca}(\text{ClO}_4)_2$) found to

enable or suppress reversible Ca plating in EC:PC^[16] have been measured by us in Figure 3e. In agreement with trends in individual EC or PC solvent,^[55] the deposition-inactive $\text{Ca}(\text{TFSI})_2$ exhibits a maximum of 6.1 mS/cm at 0.5 M (room temperature). In addition, $\text{Ca}(\text{ClO}_4)_2$ had an even higher conductivity maxima of 8.1 mS/cm at 0.7 M Ca^{2+} . Interestingly, however, the conductivities of these ‘inactive’ salts were virtually indistinguishable from the ‘active’ $\text{Ca}(\text{BF}_4)_2$ in EC:PC (maximum at 5.6 mS/cm). In other words, maximized ionic conductivity, and thus an implied maximization of mobile Ca^{2+} , appears to be a necessary but not sufficient predictor of successful plating. Moreover, higher temperatures promoted increased conductivity for both $\text{Ca}(\text{TFSI})_2$ and $\text{Ca}(\text{BF}_4)_2$ in comparable fashion (Figure 3f); $\text{Ca}(\text{TFSI})_2$ was even slightly higher than $\text{Ca}(\text{BF}_4)_2$ over the entire temperature range. Overall, the results point to a more complex role of the anion beyond just being a “ Ca^{2+} liberator” from ion pairs, raising the question of whether and how the anions play an active chemical role in systems where activity is observed.

3.2. Solvation Shell Composition: Anion-Paired or Not?

The Ca^{2+} solvation structure complexity and thermodynamics in carbonates are unique among the alkali and alkaline earth cations. As a consequence of its large ionic radius and divalence, Ca^{2+} is computed to have the highest number of solvating molecules in carbonates (6–9, typical ~8) among Li^+ , Na^+ , and Mg^{2+} (4, 4, and 5, respectively, Figure 4a) as determined via molecular dynamics, MD, simulation.^[57–60] Thus, the solvating environment surpasses others in terms of chemical complexity, yet, optimistically, also in degrees of freedom when considering possible future design of improved Ca^{2+}/Ca redox. In addition to solvation number, the total solvation strength of Ca^{2+} in a fixed set of neat or blended carbonates has been calculated^[57] to be substantially higher than its Li^+ , Na^+ , and Mg^{2+} counterparts (Figure 4b). Solvation free energies, determined by density functional quantum chemical calculations for each MD-simulated Ca^{2+} -solvent complex, ranged from -385 to -472 kcal/mol,^[57] substantially more negative than Na^+ , Li^+ , and even Mg^{2+} (-215 to -329 kcal/mol).^[58–60] While higher solvation energies do promote solubility and thus have been argued to be a desirable feature of Ca electrolytes previously,^[57] they also represent significant energy barriers that need to be overcome during Ca^{2+} reduction. Of note, in a separate study,^[61] increases in ion solvation strength of Li^+ when using high donor-number solvents (e.g., DMSO) were found experimentally and computationally to lead to an almost -600 mV shift in the Li^+/Li redox potential vs. a $\text{Me}_{10}\text{Fc}^+/\text{Me}_9\text{Fc}$ reference, compared to less-strongly solvating solvents such as acetonitrile. This point has, so far, been little-explored for Ca^{2+} , but may affect reduction potentials in conjunction with the known potential shifts due to Ca reference electrode drift reported in carbonates.^[62] In addition, there is currently a very limited picture of if, and how, such a complex solvation shell is shed during reduction. Note that it has been briefly mentioned that the higher temperatures

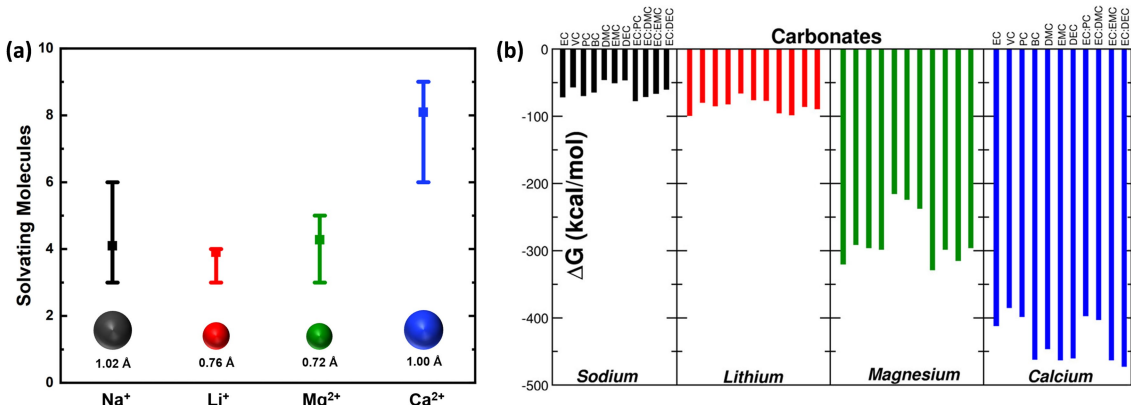


Figure 4. Complexity and strength of the Ca^{2+} solvation shell in carbonate solvents. a) Ionic radius and typical number of solvating molecules in the first solvation shell (symbol denotes average; error bars denote reported ranges across varying carbonate solvents). Data obtained from Refs. [11], [57]–[60]. Refs. [57]–[60] utilized MD simulations of 0.01 M salts in a fixed set of neat and blended carbonates; solvation numbers were determined from the primary solvation structures that were most statistically likely during computation. b) Solvation free energy of Li^+ , Na^+ , Mg^{2+} , and Ca^{2+} in acyclic and cyclic carbonates and their binary mixtures (kcal/mol_{ion}). Reprinted with permission from Ref. [57]. Copyright 2019 American Chemical Society.

used in the original EC:PC study may also aide overall desolvation kinetics.^[16,57]

The composition of the Ca^{2+} solvation environment at dilute concentrations (0.01 M) of $\text{Ca}(\text{BF}_4)_2$ was recently investigated computationally by Shakourian-Fard *et al.*^[57] Seven neat solvents (EC, PC, EMC – ethyl methyl carbonate, DMC – dimethyl carbonate, DEC – diethyl carbonate, VC – vinylene carbonate, BC – butylene carbonate) and four solvent blends (EC:PC, EC:DMC, EC:EMC, EC:DEC) were analyzed. MD simulations indicated that Ca^{2+} interacts strongly with carbonyl ($-\text{C}=\text{O}$) oxygens and more weakly with ether oxygens (Figure 5 a), in agreement with the higher basicity of oxygen in

carbonyl moieties. The cyclic carbonates EC, VC, PC, and the solvent blends EC:PC and EC:DMC had relatively less-stable solvation shells (Figure 5 b): -385 to -412 kcal/mol, vs. <-450 kcal/mol for the others. In general, more stable Ca^{2+} solvation energies tended to correlate with 2 coordinated BF_4^- anions, as well as higher proportions of linear carbonates in the solvation sphere. Intriguingly, BF_4^- was found to pair directly with Ca^{2+} even at 0.01 M; depending on the carbonate, 1–2 BF_4^- coordinated Ca^{2+} (out of typical solvation numbers of 6–9). Remarkably, this was uniquely the case for Ca^{2+} , but not Li^+ , Na^+ , and Mg^{2+} , which did not interact with their respective

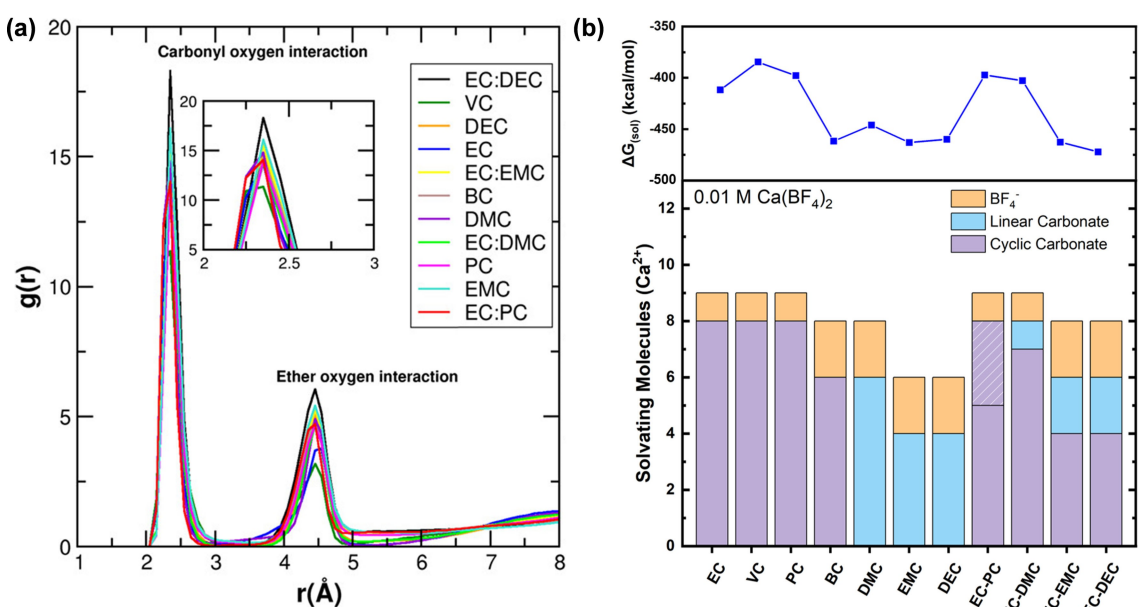


Figure 5. Ca^{2+} solvation at low concentrations (0.01 M) in carbonates. (a) Ion-oxygen radial distribution functions obtained from MD simulations. Reprinted with permission from Ref. [57]. Copyright 2019, American Chemical Society. (b) Solvation sphere composition (bottom) and free energy of solvation (top) for 0.01 M $\text{Ca}(\text{BF}_4)_2$ in carbonates. Data obtained from Table 1 within Ref. [57].

anions (PF_6^- , ClO_4^- , and ClO_4^-)^[58–60] at 0.01 M and were instead completely solvated by the carbonates.

Experimentally, Tchitchevova *et al.* utilized Raman spectroscopy to probe differences in solvation environment of Ca^{2+} and other cations in carbonates with TFSI^- .^[62] Measurements were conducted at 40 and 80 °C. Blue-shifts were observed in a cation-EC band around 900 cm⁻¹ that increased, compared to neat EC, in the order $\text{K}^+ < \text{Na}^+ < \text{Li}^+ < \text{Ca}^{2+} < \text{Mg}^{2+}$ in both EC and EC:PC (1:1), and the authors suggested that these shifts reflected increased cation-solvent interaction.^[62] At 0.1 M, negligible cation-TFSI⁻ interactions for Ca^{2+} were observed. As salt concentration increased to 1 M, Ca^{2+} -TFSI⁻ ion pairing became prevalent (Figure 6a). In EC-only, the number of EC molecules in the Ca^{2+} solvation shell decreased from 6.7 to 5.3 from 0.1 to 1 M, with the balance made up by TFSI⁻. The solvation number of the same salt at 1 M but in EC:PC had only 3.3 EC molecules in the solvation sphere, indicating some displacement by PC (Figure 6b).

Using FT-IR and Raman spectroscopy, Forero-Saboya *et al.* recently reported a detailed study of Ca^{2+} solvation environment as a function of salt concentration with finer gradation over the range 0.1–1.5 M for different carbonates.^[55] The anion was again TFSI⁻. In EC and PC, significant contact-ion pairs appeared as early as 0.5 M. In addition, by 1.2 M in both EC (Figure 6c) and PC, “free” solvent bands were almost entirely diminished, indicating a cross-over into a highly-concentrated electrolyte state. While of fundamental interest, no electrochemical activity has yet been observed with TFSI⁻.

Moving forward, expanded and consistent physico-chemical testing is needed – particularly for electrochemically-relevant electrolytes which have yet to be fully characterized – to further reveal how the Ca^{2+} solvation shell chemistry manifests in the

degree of Ca^{2+}/Ca redox reversibility. In addition, theoretical calculations have identified several potentially interesting electrolyte formulations with lower solvation strengths (Figure 5b) akin to the successful $\text{Ca}(\text{BF}_4)_2/\text{EC:PC}$ system but which have yet to be experimentally tested. Further studies are still needed to extract areal-current-density metrics in carbonates and determine whether carbonates provide a compelling path forward for future electrolyte design. This is especially so in light of recent accelerations in development of ether-based electrolytes, which can already achieve attractive current densities.

4. Successful Ca Plating and Stripping in Ether-Based Electrolytes

4.1. $\text{Ca}(\text{BH}_4)_2$ in THF with Au or Pt Electrodes

The investigation of ether-based Ca^{2+} electrolytes began in 2018 when Wang *et al.* reported highly reversible Ca plating in 1.5 M $\text{Ca}(\text{BH}_4)_2$ in THF using a gold working electrode.^[17] Under CV conditions at 25 mV/s, high areal current densities of ~10 mA/cm² were achievable with high plating capacities (~0.4 C/cm²) and a CE of 95% (Figure 7a). The electrolyte was reported to react quickly with freshly-deposited Ca to form exclusively CaH_2 in the SEI. It was indicated that the reactive electrolyte component forming CaH_2 was likely THF rather than BH_4^- based on gas chromatography-mass spectrometry measurements of THF-soaked Ca, where a $\text{C}_4\text{H}_6\text{O}$ byproduct was reported. Electrochemical measurements were attempted with $\text{Ca}(\text{TFSI})_2$ in THF but were unsuccessful. This counterintuitively

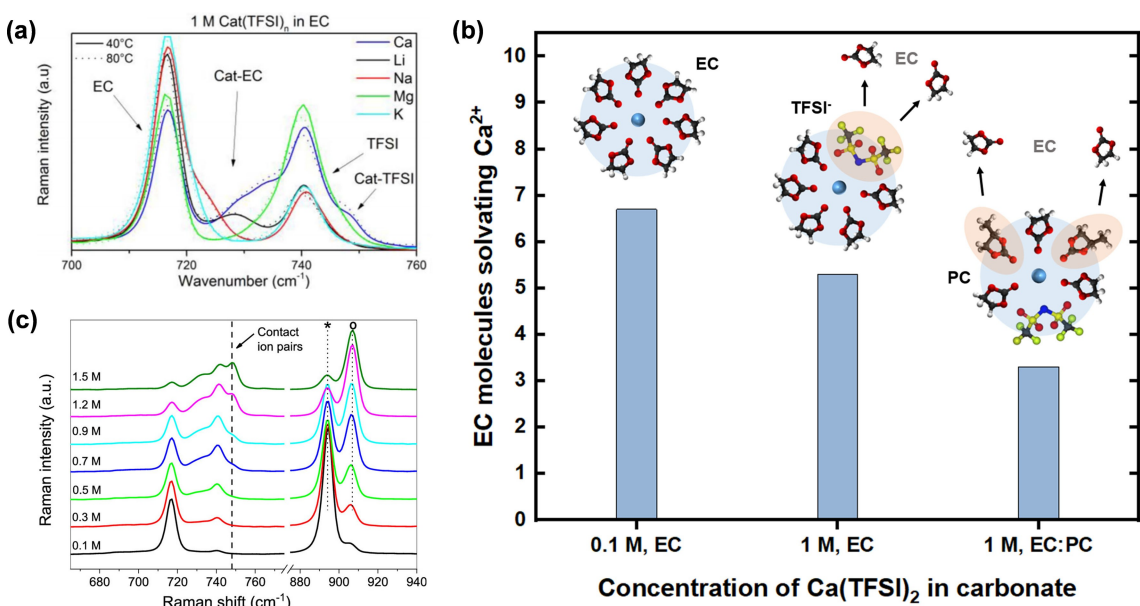


Figure 6. Spectroscopic data of Ca^{2+} solvation at moderate concentrations (0.1–1.5 M) in carbonates. a) Raman spectroscopy for 1 M TFSI⁻-based salts in EC:PC. Reprinted with permission from Ref. [62]. Copyright 2017, The Electrochemical Society. b) Number of solvating EC molecules around $\text{Ca}(\text{TFSI})_2$ in EC or EC:PC. Data obtained from Table 2 within Ref. [62]. c) Raman spectra for various concentrations of $\text{Ca}(\text{TFSI})_2$ in EC. Reprinted with permission from Ref. [55]. Copyright 2019, American Chemical Society.

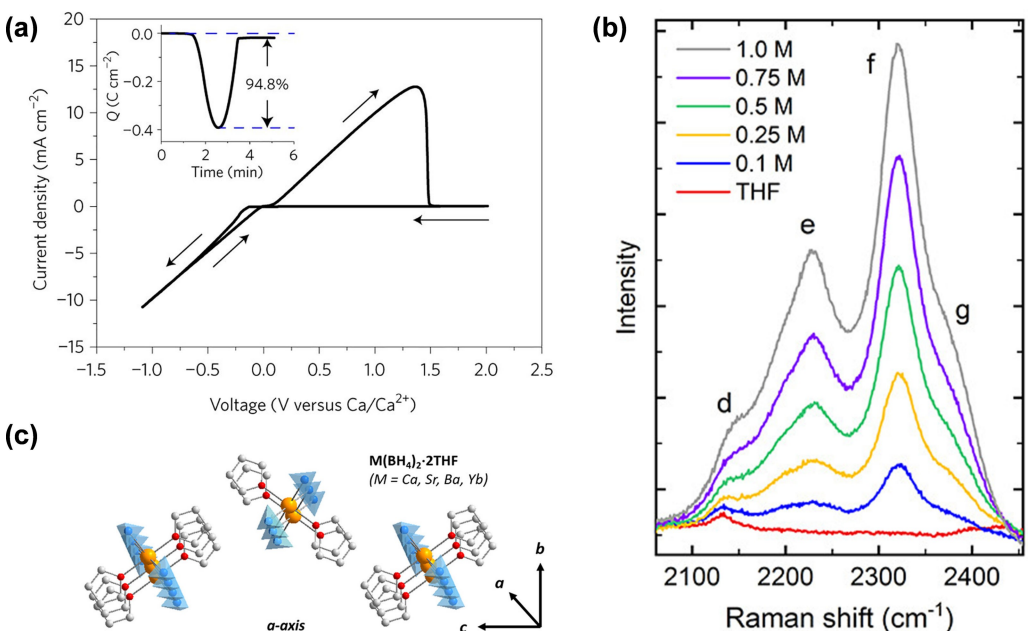


Figure 7. Performance and structure of $\text{Ca}(\text{BH}_4)_2$ as-prepared and in THF. a) CV with 1.5 M $\text{Ca}(\text{BH}_4)_2$ in THF (Au WE) at 25 mV/s. Reprinted by permission from Springer Nature: Nature Publishing Group, Nature Materials, Ref. [17], Copyright 2018. b) Raman spectroscopy of varying concentrations of $\text{Ca}(\text{BH}_4)_2$ in THF. 2226 cm^{-1} , "e", corresponds to B–H symmetric stretching. 2321 and 2373 cm^{-1} , "f" and "g", correspond to B–H asymmetric stretching. Adapted with permission from Ref. [63]. Copyright 2019 American Chemical Society. c) Crystal structure of the as-prepared $\text{Ca}(\text{BH}_4)_2\cdot 2\text{THF}$ salt. Reprinted with permission from Ref. [65]. Copyright 2018 American Chemical Society.

indicated that THF alone is insufficient to enable cycling, highlighting an apparently important role of BH_4^- even though the salt was not originally proposed to be the origin of the CaH_2 SEI.

Recently, Ta *et al.* proposed an explanation for the functional role of BH_4^- in the successful $\text{Ca}(\text{BH}_4)_2/\text{THF}$ system.^[63] Linear sweep voltammetry with ultramicroelectrodes was performed on both Au and Pt working electrodes. The authors found that Ca deposition occurs through a chemical-electrochemical mechanism, in which chemical H abstraction from BH_4^- in the bulk electrolyte (and not THF) and surface H adsorption precedes subsequent reduction of Ca^{2+} . It is important to note that, so far, Ca deposition from $\text{Ca}(\text{BH}_4)_2$ in THF has only been reported on precious metal surfaces (Au or Pt), which may be necessary for the initial H surface adsorption. In addition, Liquid Injection Field Desorption Ionization (LIFDI)-MS indicated a significant presence of $\text{BH}_3\cdot \text{THF}$ remaining in solution as evidence of the indicated abstraction. Raman spectroscopy of prepared electrolytes indicated bands at 2200–2400 cm^{-1} originating from BH_4^- stretching modes (Figure 7 b), which increased in intensity with increasing concentration (neat THF – 1 M) but did not change position. Thus, the authors concluded that Ca^{2+} is predominantly solvated by THF *via* the ethereal oxygen and is weakly coordinated, if at all, to BH_4^- .^[63] Overall, the findings point towards a surface-chemical role of the anion. Interestingly, the conductivities of $\text{Ca}(\text{BH}_4)_2/\text{THF}$ electrolytes were significantly lower than their carbonate-based counterparts (Figure 3 e). With increasing concentration from 0.1 to 1.5 M, the conductivity increased from 0.003 mS/cm to 0.71 mS/cm; no maximum was reached, as in the case of carbonates, further supporting a lack of significant ion-pairing.

In addition to basic electrolyte transport properties, it is also interesting to note the distinct qualitative differences in CV shape between $\text{Ca}(\text{BH}_4)_2/\text{THF}$ (Figure 7 a) and elevated-temperature $\text{Ca}(\text{BF}_4)_2/\text{EC}: \text{PC}$ (Figure 3 a), such as the wider oxidation peak and nearly identical slopes of the plating/stripping lines for $\text{Ca}(\text{BH}_4)_2/\text{THF}$. Understanding the origins of these distinct CV features – whether related to differences in surface film composition and SEI transport, different Ca^{2+} desolvation and redox mechanisms for ether- vs. carbonate-based electrolytes, or other – will be valuable in future experimental efforts.

4.2. Linear Ethers: High Reversibility with Simpler Solvation Shells

Two independent studies by Shyamsunder *et al.*^[31] and Li *et al.*^[32] recently reported a new Ca^{2+} salt that allows for Ca plating and stripping in 1,2-dimethoxyethane (DME, Figure 8 a–b). $\text{Ca}(\text{B(Ohfip})_4)_2\cdot 4\text{DME}$, containing the highly electron-withdrawing hexafluoroisopropoxy ligand ($\text{O}(\text{fip})^-$), was prepared by solution synthesis. The salt is analogous to a successful Mg-battery electrolyte proposed to support Mg plating/stripping due to limited ion pairing from charge delocalization in the bulky anion.^[64] In the Ca^{2+} analogue, Ca^{2+} was found to be coordinated by O atoms from structural DME molecules in the as-prepared salt (Figure 8 c), based on refinement of single-crystal X-ray diffraction data.^[31,32] (Although the as-prepared structure of $\text{Ca}(\text{BH}_4)_2\cdot 2\text{THF}$ was not reported in the original studies, it is interesting to note that Ca^{2+} is directly coordinated to O atoms of structural THF in that salt as well (Figure 7 c), which may aide in dissolution.^[65]) CV measurements by

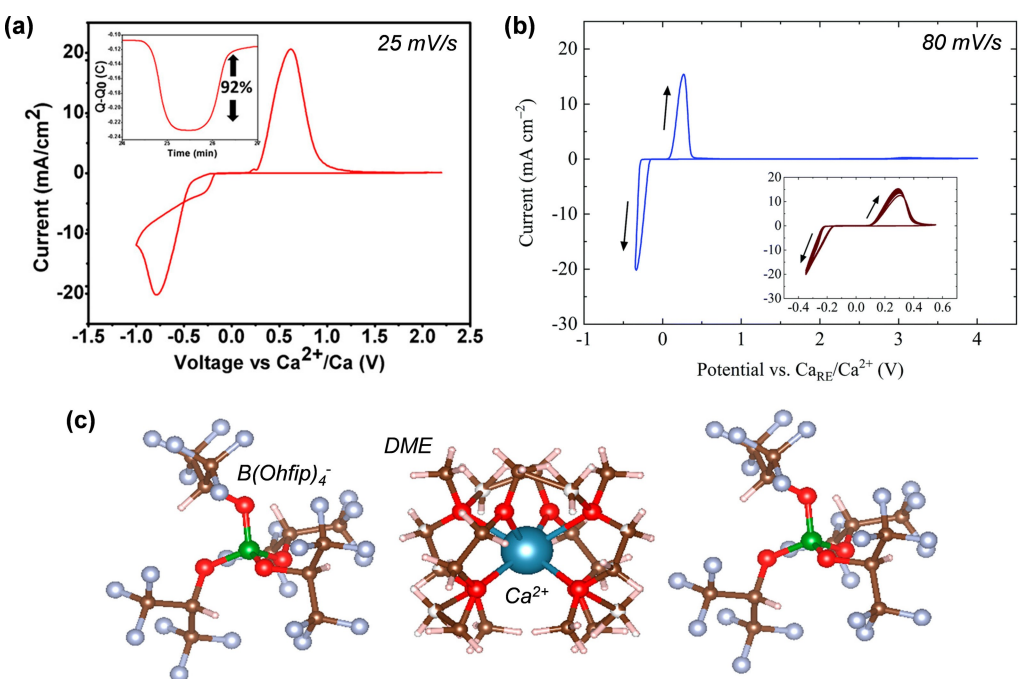


Figure 8. A new salt – $\text{Ca}(\text{B}(\text{Ohfip})_4)_2$ in DME. a) CV (4th cycle) of 0.5 M $\text{Ca}(\text{B}(\text{Ohfip})_4)_2$ in DME (Au WE, 25 mV/s).^[31] b) Cyclic voltammetry of 0.25 M $\text{Ca}(\text{B}(\text{Ohfip})_4)_2$ in DME at 80 mV/s after conditioning the Pt electrode. Inset shows cyclic voltammograms from cycles 13–22. Adapted with permission from Ref. [32]. Copyright 2019, The Royal Society of Chemistry. c) As-synthesized $\text{Ca}(\text{B}(\text{Ohfip})_4)_2 \cdot 4\text{DME}$ structures obtained by XRD refinement. Figures 8(a,c) adapted with permission from Ref. [31]. Copyright 2019, American Chemical Society.

Shyamsunder *et al.* with 0.5 M $\text{Ca}(\text{B}(\text{Ohfip})_4)_2$ /DME (Au working electrode, 25 mV/s, Figure 8a) exhibited high peak current densities (-20 mA/cm^2), roughly double that of $\text{Ca}(\text{BH}_4)_2$ /THF at the same scan rate and similar cutoff voltage, and a CE of 92% (4th cycle), which increased with cycling.^[31] After 40 cycles, total current densities decreased with cycling, which was attributed to formation of a passivation layer with time. The authors noted that during galvanostatic cycling, anion decomposition competed with Ca deposition at rates $< 0.2 \text{ mA/cm}^2$, and chemical reduction of the anion's ligands formed CaF_2 with freshly plated Ca. In addition, Ca deposition was demonstrated on copper and stainless steel substrates, with non-uniform plating similar to that on Au. Interestingly, the reduction current density of this CV (Figure 8a) peaked at $\sim -0.75 \text{ V}$ vs. Ca/Ca^{2+} and then decreased in magnitude, in contrast to those of $\text{Ca}(\text{BH}_4)_2$ /THF (Figure 7a) and elevated-temperature $\text{Ca}(\text{BF}_4)_2/\text{EC:PC}$ (Figure 3a), which peaked at their respective cutoff voltages. While the two ether-based systems' CVs share the relatively wide oxidation peaks, the $\text{Ca}(\text{B}(\text{Ohfip})_4)_2$ /DME CV exhibits a larger voltage gap between the onset of reduction and oxidation, and greater hysteresis in the reduction current compared to the $\text{Ca}(\text{BH}_4)_2$ /THF CV.

The study by Li *et al.* utilized a lower concentration of salt (0.25 M in DME) and a Pt working electrode.^[32] In comparison to the previously-mentioned 0.5 M $\text{Ca}(\text{B}(\text{Ohfip})_4)_2$ /DME,^[31] the lower-concentration electrolyte had a higher ionic conductivity of 8.3 mS/cm (vs. 3.2 mS/cm). The CV for this study (Figure 8b) had a cutoff voltage placed at $\sim -0.3 \text{ V}$, before the expected peak in reduction current density shown in the preceding study, and a higher scan rate of 80 mV/s; regardless, the peak

currents obtained on reduction ($\sim 20 \text{ mA/cm}^2$) were comparable for both studies. Increasing CE was also observed with cycling, and a moderate CaF_2 content ($\sim 7\%$) after plating was observed, similarly attributed to anion decomposition. The authors noted that the average O–Ca bond length (2.43 Å) of DME-coordinated Ca^{2+} is longer than that of Mg^{2+} in the analogous crystal (2.06 Å), and it was suggested that the desolvation energy of Ca^{2+} may thus be slightly lower than that of the Mg^{2+} in solution.

Given the successful ability of these two ether-based electrolyte systems – $(\text{BH}_4)^-$ in THF, and $\text{B}(\text{Ohfip})_4^-$ in DME – to promote reversible plating of Ca^{2+} , it is interesting to examine similarities and differences with close Mg^{2+} analogues.^[9,15] In 2012, Mohtadi *et al.* compared electroactivity of $\text{Mg}(\text{BH}_4)_2$ in both THF (0.5 M) and DME (0.1 M).^[66] While ion pairing and aggregate formation was observed in both solvents by IR and NMR spectroscopy, plating current densities and CE achieved in DME ($\sim 0.2 \text{ mA/cm}^2$, 67%) were significantly higher than those in THF (0.03 mA/cm^2 , 40%) on a Pt working electrode at 5 mV/s. The superior electrochemical performance was attributed to the higher O-donor denticity of DME (bidentate) as opposed to THF (monodentate), which results in stronger solvation of Mg^{2+} and, consequently, higher degree of dissociation of Mg^{2+} and BH_4^- . Subsequent studies^[67,68] utilizing varying chain length glymes showed a monotonic dependence of Mg plating current densities and CE with chain length, *e.g.* from 67% CE in DME to 84% in TEGDME on a Pt electrode at 20 mV/s. This was consistent with the trend of $\text{Mg}(\text{BH}_4)_2$ dissociation (confirmed via ^{25}Mg NMR and transmittance FT-IR), which increased in the order of DME < diglyme < triglyme < TEGDME. To explain the

above trends, Shao *et al.* employed MD simulations to demonstrate that longer glymes enable stronger coordination between the solvent and Mg^{2+} , which leads to increased Mg^{2+} shielding and hence weakened Mg^{2+} -anion interactions.^[67] (It is worth noting that solvation numbers, in general, with linear glymes are much lower than with carbonates given their multi-dentate solvation, leading to fewer degrees of freedom of solvation-shell modification, but perhaps simpler desolvation mechanisms overall.) Although Ca deposition experiments involving longer glymes are not yet reported, the $Ca(BH_4)_2/THF$ system is observed to have no significant cation-anion interactions^[63] with promising electrochemical performance (~10 mA/cm², 95%, at 25 mV/s).^[17] These noteworthy differences in both ion-pairing behavior and electrochemical performance of Ca^{2+} vs. Mg^{2+} in similar solvation environments (THF, BH_4^-) lends further evidence to the importance of cation/anion size, steric effects, and charge distribution in multivalent electrolyte systems.^[12,14,15] While Mg^{2+} comparisons have provided crucial inspiration for Ca^{2+} electrolyte development (*e.g.* $Mg(BH_4)_2/THF$, $Mg(B(OH)_{4})_2/DME$), the cations' fundamental differences need further careful consideration to improve the odds of successful development of Ca^{2+} analogues.

5. Summary and Future Considerations

The past several years have brought an exciting series of promising Ca electrolyte systems to the forefront, providing new research platforms to support continued study. Unlike Li anodes, the chemical environments in which Ca^{2+} can plate/stripping, even over a single cycle, are much more restrictive. Differences in the electrolyte formulations, testing conditions (different scan rates) and reliance upon precious metal electrodes (Au or Pt in many cases) makes a comprehensive analysis of the intrinsic function of most promising systems challenging at present, but this will doubtlessly be revealed with sustained experimental efforts. A common point invoked in the context of both carbonate and ether studies so far is the preliminary observation that minimizing Ca^{2+} -anion pairing may facilitate good electrochemical performance (*e.g.* increase current density and Coulombic efficiency),^[16,31,32,55] though it is clear that some ion pairing does not disqualify an electrolyte system from successful Ca deposition, as with $Ca(BF_4)_2/EC:PC$.^[16,54] It will be important to critically examine, first, whether this trend is categorically true through sustained exploration of additional electrolyte formulations and rigorous spectroscopy/computational efforts; and second, whether a causal effect can be established. In addition, the 'successful' systems reported so far should be tested on a range of electrode substrates, including C, stainless steel, etc., to screen for practical viability. More fundamental efforts into the nature of Ca^{2+}/Ca redox, including quantitative determination of redox potentials with non-reactive, yet-to-be-designed reference electrodes, will be highly valuable to further disentangle the energetics and kinetics of Ca deposition. While this mini-review has focused on electrolyte solvation structures including the anion's role, more understanding is also needed on the strongly confounding

factors of the interface's composition, structure, and properties on Ca^{2+}/Ca redox before future electrochemical measurements can be meaningfully interpreted at a mechanistic level. Overall, there is much yet to be learned about Ca^{2+} in solution and within the SEI, defining an exciting era at the intersection of electrolyte chemistry, interface study and design, and fundamental electrochemistry.

Acknowledgments

The authors gratefully acknowledge financial support from an MIT Energy Initiative SEED fund award. A.K. is supported by an MITEI Graduate Student Fellowship. For A.M.M., this work was supported by a NASA Space Technology Research Fellowship.

Conflict of Interest

The authors declare no conflict of interest.

Keywords: anode · battery · calcium · energy storage · organic electrolyte · solvent effects

- [1] J. W. Choi, D. Aurbach, *Nat. Rev. Mater.* **2016**, *1*, 16013.
- [2] R. Schmuck, R. Wagner, G. Hörpel, T. Placke, M. Winter, *Nat. Energy* **2018**, *3*, 267–278.
- [3] J. B. Goodenough, Y. Kim, *Chem. Mater.* **2010**, *22*, 587–603.
- [4] E. A. Olivetti, G. Ceder, G. G. Gaustad, X. Fu, *Joule* **2017**, *1*, 229–243.
- [5] Y. Zhao, K. R. Adair, X. Sun, *Energy Environ. Sci.* **2018**, *11*, 2673–2695.
- [6] B. Sun, P. Xiong, U. Maitra, D. Langsdorf, K. Yan, C. Wang, J. Janek, D. Schröder, G. Wang, *Adv. Mater.* **2019**, 1903891.
- [7] D. Aurbach, Z. Lu, A. Schechter, Y. Gofer, H. Gizbar, R. Turgeman, Y. Cohen, M. Moshkovich, E. Levi, *Nature* **2000**, *407*, 724–727.
- [8] P. Saha, M. K. Datta, O. I. Velikokhatnyi, A. Manivannan, D. Alman, P. N. Kumta, *Prog. Mater. Sci.* **2014**, *66*, 1–86.
- [9] R. Attias, M. Salama, B. Hirsch, Y. Goffer, D. Aurbach, *Joule* **2019**, *3*, 27–52.
- [10] A. Ponrouch, M. R. Palacín, *Curr. Opin. Electrochem.* **2018**, *9*, 1–7.
- [11] R. J. Gummow, G. Vamvounis, M. B. Kannan, Y. He, *Adv. Mater.* **2018**, *30*, 1801702.
- [12] M. E. Arroyo-de Dompablo, A. Ponrouch, P. Johansson, M. R. Palacín, *Chem. Rev.* **2019**.
- [13] W. M. Haynes, *CRC Handbook of Chemistry and Physics: 95th Edition*, CRC press, Boca Raton, 2014, p. 14–19.
- [14] P. Canepa, G. Sai Gautam, D. C. Hannah, R. Malik, M. Liu, K. G. Gallagher, K. A. Persson, G. Ceder, *Chem. Rev.* **2017**, *117*, 4287–4341.
- [15] N. N. Rajput, T. J. Seguin, B. M. Wood, X. Qu, K. A. Persson, *Top. Curr. Chem.* **2018**, *376*, 19.
- [16] A. Ponrouch, C. Frontera, F. Bardé, M. R. Palacín, *Nat. Mater.* **2015**, *15*, 169.
- [17] D. Wang, X. Gao, Y. Chen, L. Jin, C. Kuss, P. G. Bruce, *Nat. Mater.* **2017**, *17*, 16.
- [18] M. Hayashi, H. Arai, H. Ohtsuka, Y. Sakurai, *J. Power Sources* **2003**, *119–121*, 617–620.
- [19] T. Shiga, H. Kondo, Y. Kato, M. J. Inoue, *J. Phys. Chem. C* **2015**, *119*, 27946–27953.
- [20] M. Cabello, F. Nacimiento, J. R. González, G. Ortiz, R. Alcántara, P. Lavela, C. Pérez-Vicente, J. L. Tirado, *Electrochim. Commun.* **2016**, *67*, 59–64.
- [21] A. L. Lipson, S.-D. Han, S. Kim, B. Pan, N. Sa, C. Liao, T. T. Fister, A. K. Burrell, J. T. Vaughney, B. J. Ingram, *J. Power Sources* **2016**, *325*, 646–652.
- [22] T. Tojo, Y. Sugiura, R. Inada, Y. Sakurai, *Electrochim. Acta* **2016**, *207*, 22–27.
- [23] M. E. Arroyo-de Dompablo, C. Krich, J. Nava-Avendaño, N. Biškup, M. R. Palacín, F. Bardé, *Chem. Mater.* **2016**, *28*, 6886–6893.

- [24] M. Smeu, M. S. Hossain, Z. Wang, V. Timoshevskii, K. H. Bevan, K. Zaghib, *J. Power Sources* **2016**, *306*, 431–436.
- [25] N. Kuperman, P. Padiggi, G. Goncher, D. Evans, J. Thiebes, R. Solanki, *J. Power Sources* **2017**, *342*, 414–418.
- [26] A. L. Lipson, S. Kim, B. Pan, C. Liao, T. T. Fister, B. J. Ingram, *J. Power Sources* **2017**, *369*, 133–137.
- [27] D. S. Tchitchevko, A. Ponrouch, R. Verrelli, T. Broux, C. Frontera, A. Sorrentino, F. Bardé, N. Biskup, M. E. Arroyo-de Domplabio, M. R. Palacín, *Chem. Mater.* **2018**, *30*, 847–856.
- [28] K. A. See, J. A. Gerbec, Y.-S. Jun, F. Wudl, G. D. Stucky, R. Seshadri, *Adv. Energy Mater.* **2013**, *3*, 1056–1061.
- [29] P. Reinsberg, C. J. Bondue, H. Baltruschat, *J. Phys. Chem. C* **2016**, *120*, 22179–22185.
- [30] X. Yu, M. J. Boyer, G. S. Hwang, A. Manthiram, *Adv. Energy Mater.* **2019**, *9*, 1803794.
- [31] A. Shyamsunder, L. E. Blanc, A. Assoud, L. F. Nazar, *ACS Energy Lett.* **2019**, *4*, 2271–2276.
- [32] Z. Li, O. Fuhr, M. Fichtner, Z. Zhao-Karger, *Energy Environ. Sci.* **2019**, *12*, 3496–3501.
- [33] J. Muldoon, C. B. Bucur, T. Gregory, *Chem. Rev.* **2014**, *114*, 11683–11720.
- [34] H. Zhao, J. Xu, D. Yin, Y. Du, *Chem. Eur. J.* **2018**, *24*, 18220–18234.
- [35] A. Ponrouch, J. Bitenc, R. Dominko, N. Lindahl, P. Johansson, M. R. Palacín, *Energy Storage Mater.* **2019**, *20*, 253–262.
- [36] R. J. Staniewicz, *J. Electrochem. Soc.* **1980**, *127*, 782–789.
- [37] E. Peled, A. Meitav, M. Brand, *J. Electrochem. Soc.* **1981**, *128*, 1936–1938.
- [38] A. Meitav, E. Peled, *J. Electrochem. Soc.* **1982**, *129*, 451–457.
- [39] E. Peled, E. Elster, R. Tulman, J. Kimmel, *J. Power Sources* **1985**, *14*, 93–98.
- [40] C. W. Walker Jr, W. L. Wade Jr, M. Binder, S. Gilman, *J. Electrochem. Soc.* **1986**, *133*, 1555–1558.
- [41] W. L. Wade Jr, C. W. Walker Jr, M. Binder, *J. Power Sources* **1989**, *28*, 295–300.
- [42] C. W. Walker Jr, *J. Power Sources* **1989**, *25*, 13–25.
- [43] C. W. Walker Jr, *A Review of the Calcium Thionyl Chloride Electrochemical System*, Army Lab Command Fort Monmouth NJ Electronics Technology and Devices Lab, **1991**.
- [44] M. Binder, S. Gilman, W. L. Wade Jr, *J. Electrochem. Soc.* **1982**, *129*, 897–899.
- [45] E. Peled, R. Tulman, A. Meitav, *J. Power Sources* **1983**, *10*, 125–135.
- [46] C. W. Walker Jr, W. L. Wade Jr, M. Binder, *J. Electrochem. Soc.* **1988**, *135*, 2471–2472.
- [47] C. W. Walker Jr, W. L. Wade Jr, M. Binder, *J. Power Sources* **1989**, *25*, 187–193.
- [48] Y. Bedfer, J. Corset, M. C. Dhamelincourt, F. Wallart, P. Barbier, *J. Power Sources* **1983**, *9*, 267–272.
- [49] A. Meitav, E. Peled, *Electrochim. Acta* **1988**, *33*, 1111–1121.
- [50] P. Molaiyan, R. Witter, *Mater. Des.* **2019**, *1*, e44.
- [51] M. C. Verbraeken, E. Suard, J. T. S. Irvine, *J. Mater. Chem.* **2009**, *19*, 2766–2770.
- [52] D. Aurbach, R. Skalatsky, Y. Gofer, *J. Electrochem. Soc.* **1991**, *138*, 3536–3545.
- [53] A. Khurram, Y. Yin, L. Yan, L. Zhao, B. M. Gallant, *J. Phys. Chem. Lett.* **2019**, *10*, 6679–6687.
- [54] S. Biria, S. Pathreker, H. Li, I. D. Hosein, *ACS Appl. Energy Mater.* **2019**, *2*, 7738–7743.
- [55] J. D. Forero-Saboya, E. Marchante, R. Barros Neves de Araújo, D. Monti, P. Johansson, A. Ponrouch, *J. Phys. Chem. C* **2019**, *123*, 29524–29532.
- [56] M. S. Ding, K. Xu, S. S. Zhang, K. Amine, G. L. Henriksen, T. R. Jow, *J. Electrochem. Soc.* **2001**, *148*, A1196–A1204.
- [57] M. Shakourian-Fard, G. Kamath, S. M. Taimoori, J. F. Trant, *J. Phys. Chem. C* **2019**, *123*, 15885–15896.
- [58] M. Shakourian-Fard, G. Kamath, K. Smith, H. Xiong, S. K. R. S. Sankaranarayanan, *J. Phys. Chem. C* **2015**, *119*, 22747–22759.
- [59] M. Shakourian-Fard, G. Kamath, S. K. R. S. Sankaranarayanan, *ChemPhysChem* **2016**, *17*, 2916–2930.
- [60] M. Shakourian-Fard, G. Kamath, S. K. R. S. Sankaranarayanan, *ChemPhysChem* **2015**, *16*, 3607–3617.
- [61] D. G. Kwabi, V. S. Bryantsev, T. P. Batcho, D. M. Itkis, C. V. Thompson, Y. Shao-Horn, *Angew. Chem. Int. Ed.* **2016**, *55*, 3129–3134.
- [62] D. S. Tchitchevko, D. Monti, P. Johansson, F. Bardé, A. Randon-Vitanova, M. R. Palacín, A. Ponrouch, *J. Electrochem. Soc.* **2017**, *164*, A1384–A1392.
- [63] K. Ta, R. Zhang, M. Shin, R. T. Rooney, E. K. Neumann, A. A. Gewirth, *ACS Appl. Mater. Interfaces* **2019**, *11*, 21536–21542.
- [64] Z. Zhao-Karger, M. E. Gil Bardaji, O. Fuhr, M. Fichtner, *J. Mater. Chem. A* **2017**, *5*, 10815–10820.
- [65] B. Richter, J. B. Grinderslev, K. T. Møller, M. Paskevicius, T. R. Jensen, *Inorg. Chem.* **2018**, *57*, 10768–10780.
- [66] R. Mohtadi, M. Matsui, T. S. Arthur, S. J. Hwang, *Angew. Chem. Int. Ed.* **2012**, *51*, 9780–9783.
- [67] Y. Shao, N. N. Rajput, J. Hu, M. Hu, T. Liu, Z. Wei, M. Gu, X. Deng, S. Xu, K. S. Han, *Nano Energy* **2015**, *12*, 750–759.
- [68] Y. Shao, T. Liu, G. Li, M. Gu, Z. Nie, M. Engelhard, J. Xiao, D. Lv, C. Wang, J.-G. Zhang, *Sci. Rep.* **2013**, *3*, 3130.

Manuscript received: December 17, 2019

Revised manuscript received: February 13, 2020

Accepted manuscript online: February 16, 2020

Version of record online: March 19, 2020